

Title No. 112-S45

# Experimental Investigation of Prestress Losses in Full-Scale Bridge Girders

by David B. Garber, José M. Gallardo, Dean J. Deschenes, and Oguzhan Bayrak

*An experimental study was conducted in which 30 full-scale, precast, pretensioned bridge girders were constructed and instrumented with the intention of investigating prestress loss. Several different precast beam fabrication plants were used to investigate the influence of different concrete materials and construction techniques. The constructed girders were conditioned in several different climates for up to 3 years. During this period, prestress loss was measured by using vibrating wire gauges (VWG) embedded in test specimens. Following the conditioning period, the girders were flexural service load-tested to quantify the prestress loss at the time of testing and in turn verify the losses measured using VWGs. Prestress losses were found to be heavily influenced by concrete stiffness, which was dependent on coarse aggregate type and quantity. The measured short- and long-term prestress losses were compared to those determined using several different estimation procedures, suggested by ACI Committee 423.*

**Keywords:** prestress loss; prestressed bridge girder; pretensioned concrete.

## INTRODUCTION

Prestressed concrete construction relies on the application of compressive stress to concrete elements; the goal of this compressive stress being to reduce the maximum concrete tensile stresses and thus preventing cracking. The pre-compression stress (that is, prestress) is applied to the element using tendons either stressed prior to concrete placement (pretensioning) or after the concrete is allowed to harden (post-tensioning). Over time, the prestress will fluctuate due to concrete behavioral mechanisms (for example, creep and shrinkage) and external events affecting the member (such as deck placement). Any decrease in the prestress is considered prestress loss and any increase is stress gain. Stress gains are caused by elongation of the strand, typically a result of a positive moment being placed on the beam either by an external load or by the differential shrinkage of the deck; many sources elaborate on this phenomenon.<sup>1-4</sup> For the purpose of this paper, losses are positive and gains are negative.

The stress in the strand must be properly estimated throughout the life of the concrete member to ensure proper crack prevention (that is, extreme fiber concrete stress is always below the prescribed tensile stress limits), if such is desired. The stress in the prestressing strand immediately prior to transfer can be determined by monitoring the applied stress and verified by measurement of strand elongation. After the stress is transferred to the member, however, a method for estimating the prestress loss and gain is required for the designer to estimate the strand stress at different points in the life of the member.

The main factors affecting prestress loss are either related to concrete deformations (elastic shortening, creep, and shrinkage) or relaxation of the prestressing steel. As with typical deformation-related problems, the problem of concrete deformations can be approached by looking at the stresses applied on the system and the effective stiffness of the system, the system being any reinforced concrete member or structure under some type of sustained loading.

Stresses acting on concrete are primarily a result of moisture movement and externally applied stress. The movement of moisture will drive the concrete behavioral mechanism of shrinkage. Concrete creep will be driven by the externally applied stress but will also be greatly influenced by the movement of moisture. Moisture movement (primarily in relation to shrinkage) is thought to be driven by several different phenomena. While the beam is being moist- or steam-cured, the initial free water present will be partially “lost” as it is used to hydrate the cement. Once the beam is exposed to the environment, additional water will be lost through further cement hydration and as the internal system’s relative humidity equilibrates with the external ambient relative humidity. Many factors (such as cement particle size, water-cement ratio, aggregate porosity, and supplemental cementitious material type and quantity) affect the ease of the free water to move through the concrete matrix.

Prior to initial set, any free water loss will not cause any stresses to develop within the system. After cement hydration has caused the formation of the concrete matrix, further free water loss will cause the development of stress on the system, with the magnitude of these stresses primarily dependent on the pore system and the water content within the matrix. A further explanation of the shrinkage mechanism is beyond the scope of this introduction, but is fully explored by several other investigations.<sup>1,5-9</sup> While a detailed explanation of the creep mechanism is also considered to be beyond the scope of this paper, it is important to recognize that creep is also influenced by the moisture content. The mechanisms driving creep are discussed in detail by several other investigations.<sup>1,8,10-13</sup>

The stresses experienced by the system are mainly resisted by the system stiffness, which is primarily provided by the hardened cement paste and coarse aggregate. The coarse

*ACI Structural Journal*, V. 112, No. 5, September-October 2015.

MS No. S-2014-097.R3, doi: 10.14359/51687909, received September 22, 2014, and reviewed under Institute publication policies. Copyright © 2015, American Concrete Institute. All rights reserved, including the making of copies unless permission is obtained from the copyright proprietors. Pertinent discussion including author’s closure, if any, will be published ten months from this journal’s date if the discussion is received within four months of the paper’s print publication.

aggregate properties are influential in the total system stiffness: a soft coarse aggregate will generally result in a soft system. The composition of the hardened cement paste is also influential in the system stiffness; under sustained loads, the effectiveness of the hydrated cement paste to resist the stress-induced deformations will decrease with the load magnitude (dependent on the hydrated cement paste composition). Further information on long-term concrete deformations can be found in several other investigations.<sup>1,3,7,8,13</sup>

From the previous discussion on both the short- and long-term development of prestress loss, the influence of both the concrete mixture design properties and the environmental conditions becomes evident. The experimental program for this project<sup>2</sup> was designed with both of these influential factors in mind. The beams were constructed at three different precast beam fabrication plants to investigate the effect of different concrete mixture designs and properties. Some of the beams were then shipped to two different storage locations, while others were kept in the fabrication plants. In this way, five different exposure sites with different climates were employed to investigate the effect of differing environmental conditions. These specimens were monitored over time and tested after several years of storage to determine the development of prestress loss and the magnitude of the final losses. Results from these tests were used to evaluate commonly used prestress loss estimation procedures.

It should be noted that the focus of this research was on elastic shortening, creep, and shrinkage losses. Relaxation losses are dependent primarily on the type of prestressing strand used, and were not explicitly measured in this study. Relaxation is best measured on individual strands in which the strand is held at a constant strain and the stress loss is measured; this type of testing was not conducted during this research program. Because relaxation losses are strand dependent (and not necessarily system-dependent) and were not explicitly measured in this study, the treatment of these losses elsewhere<sup>4,14</sup> is sufficient.

## RESEARCH SIGNIFICANCE

The main advantage of prestressed concrete is the prevention of service-load cracking through the application of a pre-compression stress (that is, prestress) in the flexural tension zone. Losses in pre-compression undoubtedly reduce the efficiency of prestressed concrete. The prevention of service-load cracking is dependent on the designer's ability to conservatively and precisely estimate this stress throughout the life of the girder. The research reported in this paper is significant as it is one of the largest studies (in both specimen size and quantity) ever conducted investigating prestress loss. Several different loss measurement techniques and the most influential variables were investigated and are reported in this paper.

## EXPERIMENTAL INVESTIGATION

In total, 30 full-scale prestressed concrete beams were fabricated, conditioned, and tested to enable comprehensive assessment of short- and long-term prestress losses. The specimens were representative of a broad range of the most influential factors affecting prestress losses including:

concrete materials used, prestress level, specimen geometry, fabrication techniques, and climate conditions.

## Specimen design and material properties

The 45.5 ft (13.9 m) long specimens were either Type C (40 in. [1016 mm] deep standard AASHTO I-girder) or Tx46 (46 in. [1168 mm] deep bulb-T) cross sections, as shown in Fig. 1(b) and (c); these sections represent commonly used sections in past and current practices, respectively. The girders were designed to maximize the compressive stress ratio at release to near  $0.65f_{ci}'$  while satisfying AASHTO tensile stress limits. Although this compressive stress ratio is larger than the limit of  $0.60f_{ci}'$  found in ACI 318-14 (Section 18.4.1),<sup>15</sup> higher compressive stress ratios of  $0.65f_{ci}'$  and higher are commonly used in bridge design.<sup>16</sup> This design criterion led to the strand patterns and harping scheme depicted in Fig. 1. End region and shear reinforcement was detailed per the TxDOT Design Specification.<sup>17</sup> A summary of the relevant specimen properties is presented in Table 1.

The concrete mixture proportions are summarized in Table 2. The concrete mixture designs were chosen based on commonly used mixtures at the three different precast facilities chosen for specimen fabrication. The type and quantity of the coarse aggregate used was one of the main differences between the mixture designs. Two different coarse aggregate types were used: a softer crushed limestone (Series I and III in Table 2) and stiffer river gravel (Series II and IV in Table 2). The self-consolidating concrete (SCC) in Series IV used a lower coarse aggregate content (1540 lb/yd<sup>3</sup> [914 kg/m<sup>3</sup>] for SCC versus 1780 lb/yd<sup>3</sup> [1056 kg/m<sup>3</sup>] for conventional concrete [CC]) and a higher fines content (930 lb/yd<sup>3</sup> [552 kg/m<sup>3</sup>] of cement and fly ash for SCC versus 820 lb/yd<sup>3</sup> [486 kg/m<sup>3</sup>] for CC). The mixture designs were fairly similar otherwise.

To properly model the behavior of the elements, the modulus of elasticity  $E_p$  and the initially applied prestressing stress  $f_{pr}$  were measured, as presented in Table 3. The initially applied prestressing stress was found by measuring the elongation of the strand and monitoring the applied stress from the hydraulic jack.

The hardened concrete material properties were also required for three different times: at the time of prestress transfer or release ("At Release"), 28 days after the beams were cast ("28 Days"), and at the time of flexural service load testing ("At Test"). The concrete compressive strength  $f_c$ , modulus of elasticity  $E_{ci}$ , and tensile strength obtained from a split cylinder test  $f_{sp}$  were measured at each of the three significant times. A summary of the relevant tested concrete properties is presented in Table 4.

After the girders were fabricated, they were sent to one of four different conditioning sites: Austin, Elm Mott, Lubbock, or San Antonio (all in Texas). These sites were chosen to capture several different climates; Lubbock being significantly drier than the other three sites. The storage locations for all specimens is summarized in Table 5. A photograph of the Austin and Lubbock storage sites with girders from Series I, II, and III is provided in Fig. 2.

**Table 1—Relevant section properties for specimens in Series I through IV**

Series	$f_{ci}'$ -design, ksi	Strand diameter, in.	$A_{ps}$ , in. <sup>2</sup>	$y_{p,mid}$ , in.	Beam type	$y_b$ , in.	$A_g$ , in. <sup>2</sup>	$I_g$ , in. <sup>4</sup>	$V/S$ , in.
I	6.20	0.5	5.81	6.63	C	17.1	495	82600	3.96
II	6.20	0.5	5.81	6.63					
III	6.50	0.5	8.87	6.43	Tx46	20.1	761	198100	3.86
IV-SCC	6.05	0.5	8.57	6.64					
IV-CC	6.05	0.5	8.57	6.64					

Notes: 1 ksi = 6.9 MPa; 1 in. = 25.4 mm; 1 in.<sup>2</sup> = 645 mm<sup>2</sup>; 1 in.<sup>4</sup> = 416,000 mm<sup>4</sup>.

**Instrumentation**

Girders were instrumented using internal instrumentation—vibrating wire gauges (VWGs), shown in Fig. 3—to monitor the prestress loss over time. A VWG consists of a length of steel wire attached between two end blocks; the wire is enclosed and free to deform with the movement of the end blocks. When embedded in concrete, the VWG can be used to measure concrete strain; the wire in the gauge is plucked electromagnetically and the change in the resonant frequency of its response indicates the change in strain of the wire, which is the same as the surrounding concrete. It should be noted that only strain-related stress changes are captured by VWGs (that is, strand relaxation is not directly captured).

VWGs were typically placed at three different levels in the cross section at midspan of the beam (Fig. 1(b)) to allow for a linear strain distribution in the cross section to be measured, as shown in Fig. 4. The strain in the concrete at the centroid of the prestressing stands (equivalent to the strain in the strand itself) could be determined through linear interpolation using the linear strain profile. By systematically taking measurements over the life of the beam, the stress in the strand could be monitored over time. The prestress loss could be determined with the knowledge of the initially applied stress ( $f_{pt}$ ), shown in Table 3. A VWG measurement was also taken immediately prior to flexural service load testing to provide a comparison between the two loss measurement methods. A relaxation loss estimate (obtained

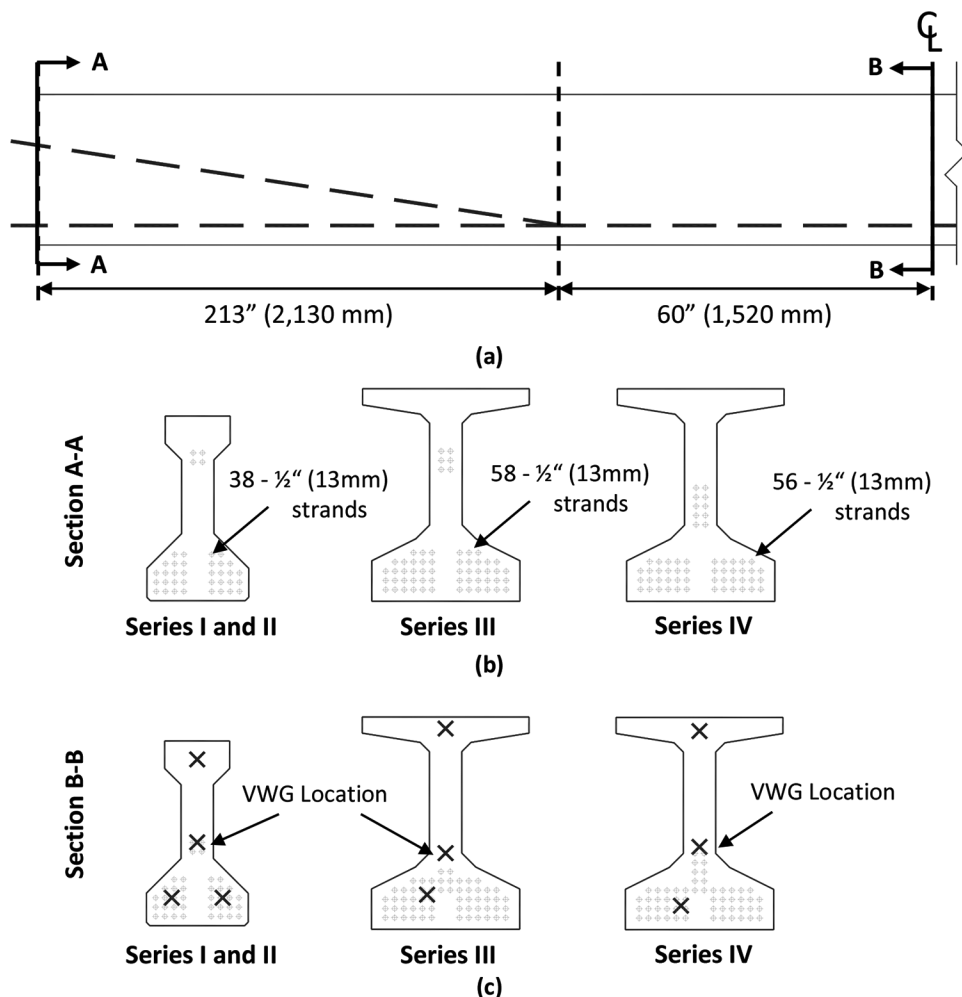


Fig. 1—Cross-sectional details: (a) harping; (b) end section; and (c) midspan section.

**Table 2—Typical concrete mixture proportions**

Material	Quantity				
	Series I	Series II	Series III	Series IV	
				SCC	CC
Type III portland cement, lb/yd <sup>3</sup>	540	530	660	700	600
Fly ash, lb/yd <sup>3</sup>	170	170	220	230	200
CA, lb/yd <sup>3</sup>	1850 (3/4 in. crushed limestone)	1970 (3/4 in. river gravel)	1850 (3/4 in. crushed limestone)	1540 (1/2 in. river gravel)	1780 (1/2 in. river gravel)
FA: Sand, lb/yd <sup>3</sup>	1220	1310	1030	1240	1220
Water, lb/yd <sup>3</sup>	180	115	180	270	220
HRWRA, oz/yd <sup>3</sup>	33	50	18	37	36
Set-retardant admixture, oz/yd <sup>3</sup>	31	14	44	9	12
Water-cement ratio	0.34	0.22	0.27	0.39	0.37
CNI admixture, oz/yd <sup>3</sup>	—	—	—	115	144
Viscosity-modifying admixture, oz/yd <sup>3</sup>	—	—	—	15	—

Notes: CC is conventional concrete; SCC is self-consolidating concrete; 1 lb/yd<sup>3</sup> = 0.6 kg/m<sup>3</sup>; 1 oz/yd<sup>3</sup> = 38.7 mL/m<sup>3</sup>.

**Table 3—Summary of measured prestressing strand information**

Series	$E_p$ , ksi (MPa)	$f_{pb}$ , ksi (MPa)
I	28,800 (199,000)	202.9 (1399)
II	28,800 (199,000)	203.0 (1400)
III	28,800 (199,000)	209.0 (1441)
IV	29,000 (200,000)	202.5 (1396)

using the AASHTO detailed method<sup>18</sup>) was added to the final loss measured by VWGs to provide a direct comparison between the service load testing (which measures losses, including relaxation) and VWG measurement (which does not include relaxation).

### Service load testing procedure

All of the specimens were subjected to flexural service load testing to determine the load required to cause initial cracking in the specimens. The cracking moment is affected by the tensile capacity of the concrete and the stress in the strands at the time of testing. The tensile strength of the concrete was measured immediately prior to testing, and the cracking moment determined through the flexural service load test allowing the prestress force in the strand (and the prestress loss) to be calculated for using the known information.

The specimens were tested using a four-point load setup capable of applying 800 kip (3560 kN) of force, as shown in Fig. 5. Load was applied through a double-acting hydraulic ram and measured using a load cell of appropriate capacity and verified with an oil pressure transducer. A region with constant moment was created at midspan using a 67 in. (1700 mm) transfer beam; cracking occurred within this constant moment region and allowed for the theoretical

strand stress to be easily determined. Displacements were measured using linear potentiometers at midspan (on both sides of the beam) and at each support (to measure support settlement). During testing, load was applied at a rate of approximately 0.5 kip (2.2 kN) per second up to approximately 75% of the estimated cracking load. Thereafter, additional load was applied in 10 kip (44 kN) increments; the beam was visually inspected for cracking in between each load increment. Once cracking was visually observed, additional load was applied in increments between 20 and 50 kip (89 and 220 kN) until extensive cracking occurred.

Although an approximate cracking load was obtained through visual inspection during testing, a better estimate was desired to calculate a more accurate prestress loss value at the time of testing. A better estimate for the cracking load could be determined using the measured load-deflection data for each test, as shown in Fig. 6(a). By discretizing the load-deflection data, the stiffness could be determined for each step. A moving average was calculated at each deflection by calculating the average of all stiffness values less than or equal to the current deflection. First cracking in the beam (the cracking point) was assumed to occur when the concrete stiffness began to significantly decrease as compared to the moving average, as shown in Fig. 6(b). This method proved to be both an accurate and repeatable method for determining the point of first cracking and also eliminated nearly all subjectivity.

It should be noted that the tensile strength was measured using split cylinder testing, which is traditionally thought to slightly underestimate the tensile strength, rather than modulus of rupture tests. This was done as the researchers deemed that the local tensile strength of concrete captured by the split cylinder test better represented the cracking load determined by the aforementioned stiffness method.

**Table 4—Summary of tested concrete properties**

Series	At release				28 days		At test		
	Age, days	$f'_{ci,design}$ , ksi	$f'_{ci,measured}$ , ksi	$E_{ci,design}$ , ksi	$E_{ci,measured}$ , ksi	$f'_{c,design}$ , ksi	$f'_{c,measured}$ , ksi	$f'_{c,measured}$ , ksi	$f_{sp,test}$ , ksi
I	1.08	6.20	7.0	4800	4490	8.5	10.7	10.6	0.83
II	0.98	6.20	6.6	4800	6140	8.5	11.6	12.7	1.00
III	1.77	6.50	6.6	4900	3990	8.5	9.6	11.8	0.91
IV-SCC	0.74	6.05	6.3	4716	4810	12	11.5	15.0	1.06
IV-CC			6.9		5440		12.0	14.1	1.06

Note: 1 ksi = 6.9 MPa.

**Table 5—Summary of prestress loss assessments**

	Storage location (RH)	Beam ID	Elastic shortening, ksi		Final age, days	Final loss, ksi			
						P-Δ	VWG	Reported	
SERIES I	Lubbock (52%)	I-1	26		980	57	46	46	Avg.
		I-5	27		975	51	51	51	49
		I-6	n/a		973	56	n/a	56	
	Austin (63%)	I-2	n/a	Avg.	939	49	n/a	49	Avg.
		I-3	26	27	948	49	46	46	47
		I-7	27		946	50	49	49	
	San Antonio (64%)	I-4	n/a		962	41	n/a	41	Avg.
		I-8	n/a		966	50	n/a	50	46
SERIES II	Lubbock (51%)	II-1	16		955	31	32	32	Avg.
		II-5	n/a		952	24	n/a	24	29
		II-6	17		949	43	36	36	
	Austin (63%)	II-2	n/a	Avg.	922	39	n/a	39	Avg.
		II-3	17	17	932	42	34	34	34
		II-8	16		923	43	33	33	
	Elm Mott (63%)	II-4	n/a		936	32	n/a	32	Avg.
		II-7	n/a		937	24	n/a	24	28
SERIES III	Lubbock (49%)	III-1	29		695	55	58	58	Avg.
		III-5	29		703	56	58	58	55
		III-8	n/a		700	54	n/a	54	
	Austin (61%)	III-3	29	Avg.	677	55	54	54	Avg.
		III-4	n/a	29	675	54	n/a	54	53
		III-7	29		681	55	53	53	
	San Antonio (63%)	III-2	n/a		689	54	n/a	54	Avg.
		III-6	n/a		687	56	n/a	56	55
SERIES IV	Austin (57%)	IV-SCC1	22	Avg.	249	48	43	43	Avg.
		IV-SCC2	22	22	259	54	42	42	40
		IV-SCC3	22		230	n/a	43	43	
		IV-CC1	21	Avg.	237	42	39	39	Avg.
		IV-CC2	20	21	257	41	38	38	36
		IV-CC3	22		251	46	40	40	

Note: 1 ksi = 6.9 MPa.

## EXPERIMENTAL RESULTS AND DISCUSSION

### Prestress loss development

Prestress loss was measured using internal VWGs to monitor the development of loss over time, which will be

presented first; VWGs also allowed for the measurement of “final” prestress loss, which will be presented in the following section. The time development of the prestress losses is shown in Fig. 7 in the form of a time-development factor



(a)



(b)

Fig. 2—Two primary beam storage sites: (a) Austin, TX; and (b) Lubbock, TX.

( $K_T$ ) versus time. The plotted time-development factor is the measured prestress loss at time  $t$  normalized by the measured loss at a time of 365 days. The normalized measured loss is plotted in Fig. 7 for all of the specimens with VWGs. A logarithmic regression, generally suggested for concrete creep development models,<sup>1,15,19</sup> seemingly represents the development of the long-term loss well, as shown in Fig. 7(b). Using the general trend of the observed loss development (that is, the logarithmic regression), approximately 90% of the 1-year prestress loss developed in the first 4 months.

Although prestress losses are shown to follow a logarithmic trend for ages of less than 3 years, further monitoring should be conducted before such a relationship is extrapolated to estimate final design life losses. Additionally, it has been suggested that losses will eventually stop increasing when the concrete stress at the strand centroid reaches zero,<sup>4</sup> which may occur as the beam ages under load in the field.

### Final prestress loss

The elastic shortening  $\Delta f_{pES}$  and total final prestress losses  $\Delta f_{pt}$  for all test specimens are presented in Table 5. Within Table 5, specimens are grouped by series and storage locations, and prestress losses are reported from both flexural service load testing and VWG measurements. Losses determined using VWG measurements were generally found to be more consistent and were thus used as the final reported loss when available. The final measured loss seems to be affected by the ambient relative humidity in most cases and by the coarse aggregate type in all cases.

As previously mentioned, ambient relative humidity (RH) is typically thought to influence the development of prestress loss by affecting the water transfer rate between specimen and environment. It is generally accepted that a higher relative humidity will result in less water loss from the specimen to equilibrate internal and external relative humidity. A smaller water loss will typically result in smaller long-term concrete deformations and a lower magnitude long-term prestress loss (for times within the design life).

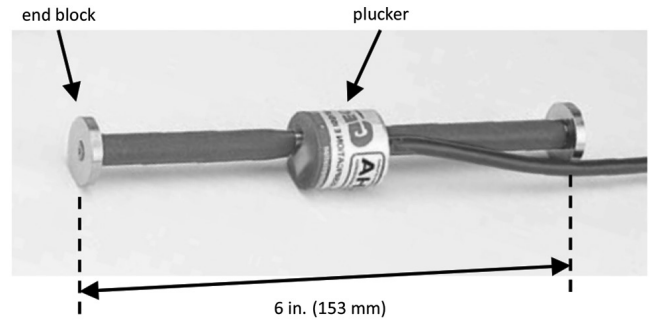


Fig. 3—Vibrating wire gauge used for instrumentation.

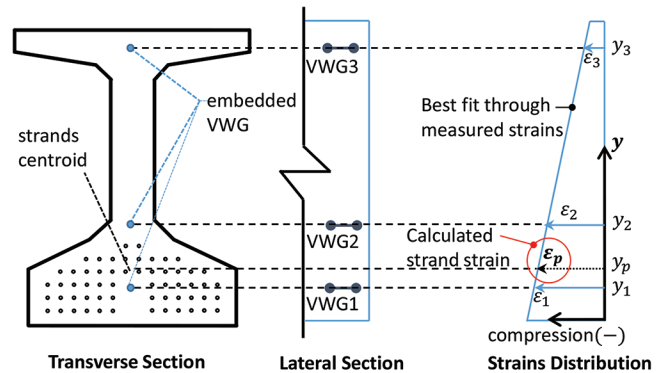


Fig. 4—Method for determining strain in prestressing strand from VWG measurements.

The average measured long-term prestress loss ( $\Delta f_{pLT}$ ) for all test specimens in Series I, II, and III are shown in Fig. 8; specimens are grouped by series and ambient relative humidity during conditioning. The average relative humidity for specimens stored in Lubbock was approximately 50%; those stored in Austin, Waco, and San Antonio had an average relative humidity of approximately 63%.

For specimens in Series I and III, specimens stored in a drier climate (52 and 49% relative humidity) experienced larger magnitude long-term losses compared to those stored in the more humid climate (63 and 62% relative humidity). Unlike Series I and III, in Series II, the ambient relative humidity had little effect on the magnitude of the long-term prestress losses. The main difference between the specimens of Series I and III and those in Series II was the coarse aggregate type. It has been previously shown that the aggregate porosity will influence the permeability of the concrete matrix.<sup>20</sup> This increased permeability in the specimens with the limestone coarse aggregate would have allowed easier moisture movement, leading to a larger loss in free water, and thus larger creep and shrinkage strains.

In addition to its influence of relative humidity effects, the coarse aggregate is thought to affect losses as it influences the ability of the concrete to restrain internally developed and externally applied stresses (through influencing the elastic modulus). Both the average elastic shortening and average long-term prestress losses for each series are presented in Table 4 and Fig. 9. In Fig. 9, the series are paired together based on the coarse aggregate used: Series I and III having limestone and Series II and IV having river gravel coarse aggregate.

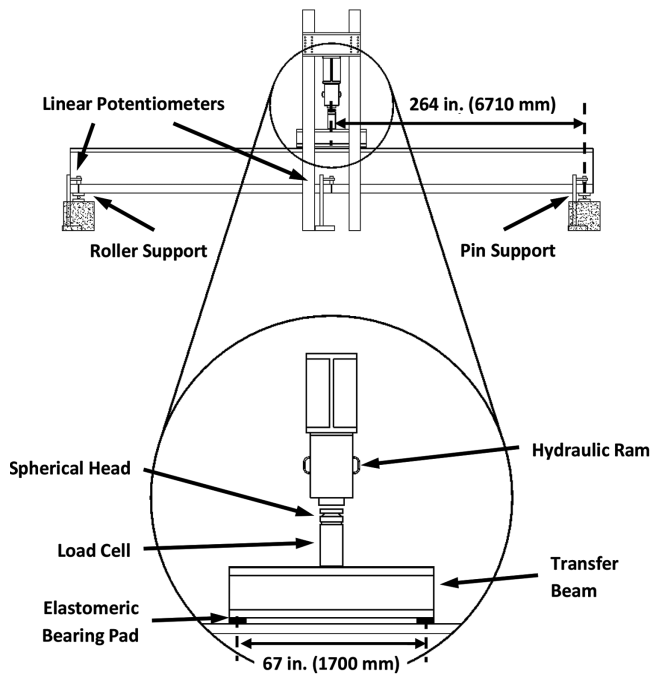


Fig. 5—Schematic of flexural test setup.

The measured modulus of elasticity at time of release ( $E_{ci}$ ) for each series is presented below the series label. The specimens constructed using limestone coarse aggregate (Series I and III) were softer than those with river gravel coarse aggregate (Series II and IV), as seen by comparing the respective moduli at release (4.5 and 4.0 ksi [31.0 and 27.6 MPa] for the Series I and III limestone specimens and 6.1 and 5.1 ksi [42.1 and 35.2 MPa] for Series II and IV river gravel specimens, respectively).

As shown in Fig. 9, both the elastic shortening  $\Delta f_{pES}$  and long-term prestress losses were influenced by the coarse aggregate type, primarily a result of the coarse aggregate's effect on the modulus of elasticity. Long-term losses were found to be on average 42% larger for similar limestone specimens compared to their river gravel counterparts. Similarly, elastic shortening losses were found to be on average 45% larger for limestone compared to river gravel specimens.

### Flexural testing versus internal strain measurements

Prestress losses were measured using both flexural service load testing and internal strain measurement techniques. Within the flexural service load testing program several different methods were investigated for determining the load required to cause first cracking. These methods included:

- Visual inspection;
- Nondestructive testing technique (impact echo technique);
- Manual load-deflection plot inspection;
- Stiffness-deflection procedure;
- Crack reopening test—load-deflection analysis; and
- Crack reopening test—concrete surface gauges.

The method based on the stiffness-deflection plots was the only method that produced both 1) consistent results among similar specimens; and 2) losses comparable to VWG readings.

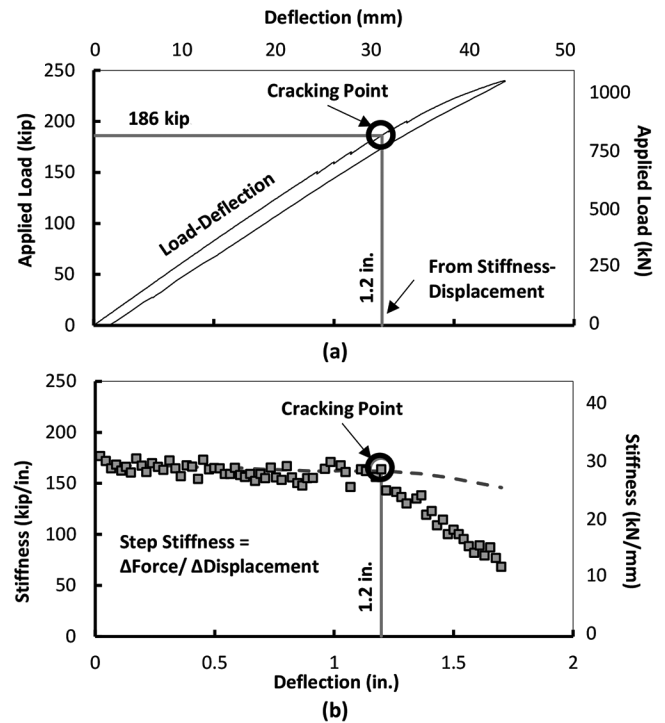


Fig. 6—Procedure for determining cracking load using both (a) applied load versus deflection plot; and (b) stiffness versus deflection plot.

By using both VWG readings and the flexural service load testing, both methods could be verified and compared with each other. The average measured prestress loss for each series is presented in Fig. 10 for both VWG measurements and flexural service load testing. When a reliable method is used to determine the cracking moment, measured prestress loss compares well with VWG measurements.

### Comparison with existing prestress loss estimation methods

As mentioned in the introduction, prestress loss must be both conservatively and precisely estimated to ensure a beam is efficiently designed and will not crack under routine service loads. To investigate the conservativeness and precision of current prestress loss estimation procedures, prestress loss was estimated for each of the specimens using the methods proposed in ACI 423.10 (ACI 423.10 is currently under development as of the writing of this study). Within this document, estimation methods are presented for both short- and long-term losses; long-term losses are recommended to be estimated using lump sum, simplified, or detailed methods depending on the situation.

Recommendations are also provided for the estimation of the modulus of elasticity of concrete. In the United States, there are primarily two expressions considered: 1) ACI 318<sup>15</sup> (Eq. (1), units in psi); and 2) AASHTO LRFD<sup>18</sup> (Eq. (2), units in ksi). The estimation procedure used for modulus of elasticity in AASHTO LRFD permits for the stiffness to be modified (using the  $K_1$  factor) based on any known information about the concrete to be used in casting. This factor is the only piece of the loss expressions compared in

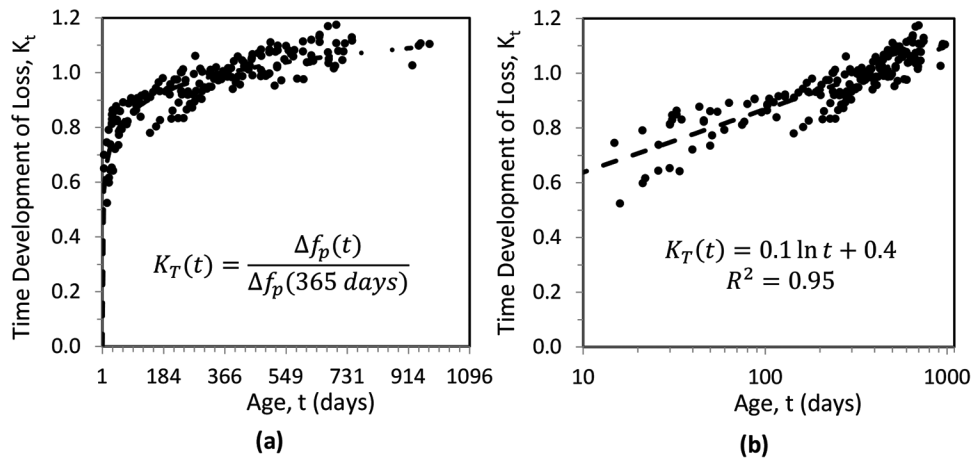


Fig. 7—Time development of prestress loss for all specimens normalized by the loss at 365 days on (a) normal; and (b) logarithmic scale.

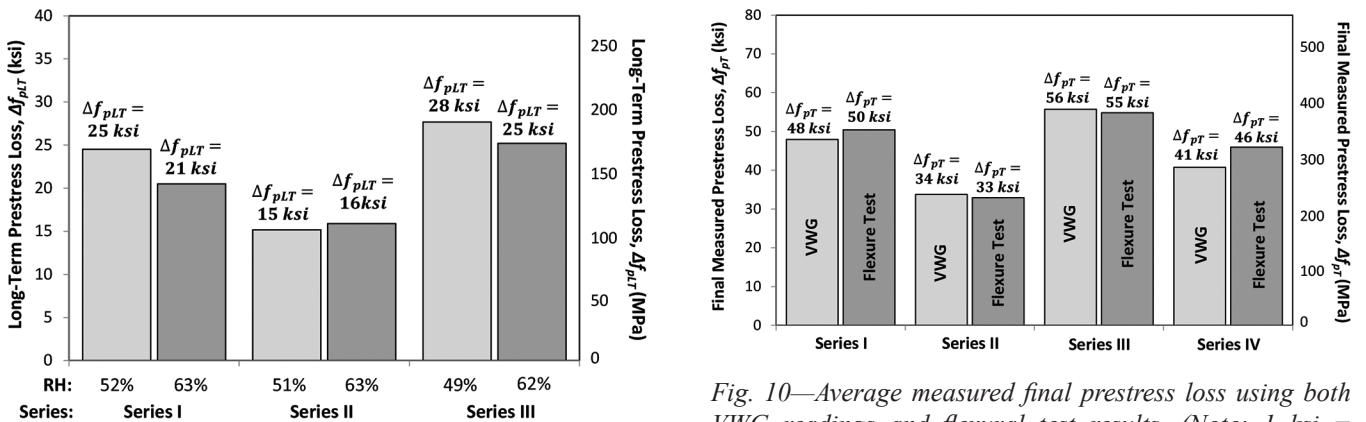


Fig. 8—Measured long-term prestress loss for test specimens separated by ambient relative humidity during conditioning. (Note: 1 ksi = 6.9 MPa.)

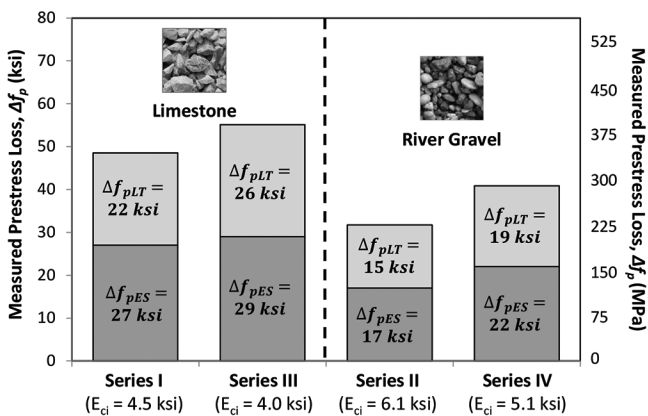


Fig. 9—Measured elastic shortening and long-term prestress loss for test specimens separated by coarse aggregate type. (Note: 1 ksi = 6.9 MPa.)

the following, in which the coarse aggregate properties may be accounted.

$$E_c = 33w_c^{1.5} \sqrt{f'_c} \text{ (units in psi)} \quad (1)$$

Fig. 10—Average measured final prestress loss using both VWG readings and flexural test results. (Note: 1 ksi = 6.9 MPa.)

$$E_c = 33,000K_1w_c^{1.5} \sqrt{f'_c} \text{ (units in ksi)} \quad (2)$$

During the following investigations, the performance of each procedure is presented by normalizing the estimated prestress loss by the measured loss ( $E/M$ ); an  $E/M$  greater than 1.0 is conservative. Specimens are divided by series for all procedure evaluations. As relative humidity is used in most long-term loss estimation methods, specimens are also divided by storage location for the long-term loss investigation.

Three different methods for estimating elastic shortening loss are suggested for use by ACI 423.10: 1) a transformed section approach; 2) gross section approach; and 3) iterative gross section approach. All three of these methods involve the basic mechanics relationship relating the stress in the concrete at the centroid of the prestressing strands  $f_{cgp}$  to the change in stress of the prestressing strands  $\Delta f_{pES}$  using the modular ratio  $E_p/E_{ci}$ , as shown in Eq. (3). The transformed section approach, shown in Eq. (4), uses the initial strand stress just before transfer  $f_{pt}$  and the transformed area  $A_t$ , strand eccentricity  $e_{pt}$ , and moment of inertia  $I_t$  to find the stress in the concrete at the centroid of the prestressing strands directly.

$$\Delta f_{pES} = E_p \epsilon_p = \frac{E_p}{E_{ci}} f_{cgp} \quad (3)$$

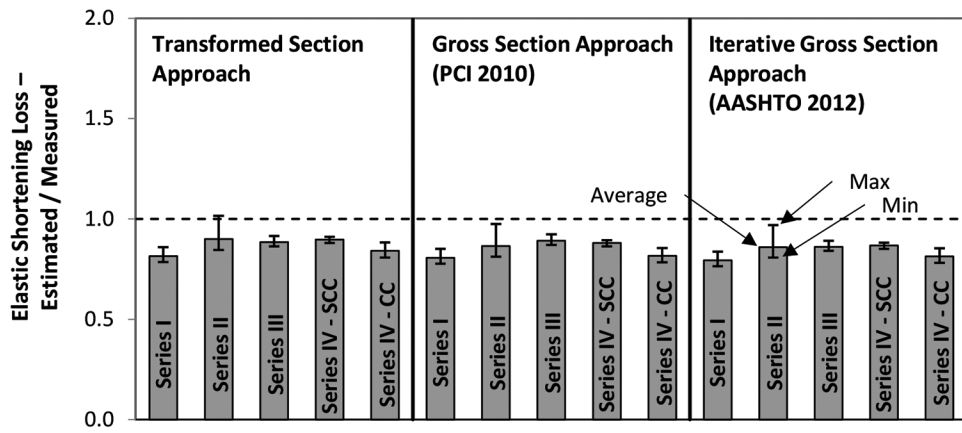


Fig. 11—E/M for elastic shortening losses measured in each series.

**Table 6—Lump-sum approach using PCI-Simplified<sup>21</sup> method**

Component	Equations
Creep	$\Delta f_{pCR} = K_{cr} \left( \frac{E_p}{E_c} \right) (f_{clr} - f_{cds})$
	$f_{cds} = \frac{M_g e_p}{I_g}$
Shrinkage	$\Delta f_{pSH} = (8.2 \times 10^{-6}) K_{sh} E_p \left( 1 - 0.06 \frac{V}{S} \right) (100 - RH)$
Relaxation	$\Delta f_{pRE} = [K_{re} - J(\Delta f_{pES} + \Delta f_{pSH} + \Delta f_{pCR})] C$

$$f_{cgp} = f_{pt} A_{ps} \left( \frac{1}{A_t} + \frac{e_{pt}^2}{I_t} \right) - \frac{M_g e_{pt}}{I_t} \quad (4)$$

This stress at the centroid of the prestressing strands can also be found directly using the gross section approach,<sup>21</sup> shown in Eq. (5), which estimates the stress in the strand after transfer to be 90% of that before ( $0.9f_{pt}$ ) and uses the gross area  $A_g$ , strand eccentricity  $e_p$ , and moment of inertia  $I_g$ .

$$f_{cgp} = 0.9 f_{pt} A_{ps} \left( \frac{1}{A_g} + \frac{e_p^2}{I_g} \right) - \frac{M_g e_p}{I_g} \quad (5)$$

The iterative gross section approach can also be used to determine the elastic loss. As its name would suggest, this method is used to obtain the final stress at the centroid of the prestressing strands and elastic shortening through an iterative process, which is described elsewhere.<sup>2</sup> This procedure can also be represented by the expression shown in Eq. (6). Use of this expression will estimate the elastic shortening loss directly using the strand stress immediately prior to transfer ( $f_{pt}$ ).

$$\Delta f_{pES} = \frac{A_{ps} f_{pt} (I_g + e_m^2 A_g) - e_m M_g A_g}{A_{ps} (I_g + e_m^2 A_g) + \frac{A_g I_g E_{ci}}{E_p}} \quad (6)$$

**Table 7—Lump-sum approach using AASHTO Approximate<sup>18</sup> method**

Equations
$\Delta f_{pLT} = 10.0 \frac{f_{pt} A_{ps}}{A_g} \gamma_h \gamma_{st} + 12.0 \gamma_h \gamma_{st} + \Delta f_{pRE}$
$\gamma_h = 1.7 - 0.01RH$
$\gamma_{st} = \frac{5}{1 + f'_{ci}}$

**Table 8—Detailed approach using AASHTO Detailed<sup>18</sup> method for before deck placement long-term losses**

Component	Equations
Total long-term creep	$\Delta f_{pLT} = (\Delta f_{pSR} + \Delta f_{pCR} + \Delta f_{pR1})_{id}$
	$\Delta f_{pCR} = \frac{E_p}{E_{ci}} f_{cgp} K_{id} \Psi_b(t_j, t_i)$
	$K_{id} = \left[ \frac{1}{1 + \frac{E_p A_{ps}}{E_{ci} A_g} \left( 1 + \frac{A_g e_p^2}{I_g} \right) (1 + \chi \Psi_b(t_j, t_i))} \right]$
	$\Psi(t, t_i) = 1.9 k_{vs} k_{hc} k_f k_{id} t^{-0.118}$
	$k_{vs} = 1.45 - 0.13(V/S) \geq 0$
	$k_{hc} = 1.56 - 0.008RH$
	$k_f = \frac{5}{1 + f'_{ci}}$
Shrinkage	$k_{id} = \frac{t}{61 - 4f'_{ci} + t}$
	$\Delta f_{pSR} = \epsilon_{bid} K_{id} E_p$
	$\epsilon_{bid} = k_{vs} k_{hs} k_f k_{id} 0.48 \times 10^{-3}$
Relaxation	$k_{hc} = 2.0 - 0.014RH$
	$\Delta f_{pR1} = \frac{f_{pt}}{K_L} \left( \frac{f_{pt}}{f_{py}} - 0.55 \right)$

**Table 9—Detailed approach using Time-Step method**

Step	Process
Step 1:	Calculate the increment of creep and shrinkage for the time step Determine: $\psi(t_{n-1}, t_0), \psi(t_n, t_0), \epsilon_{sh}(t_{n-1}), \epsilon_{sh}(t_n)$
Step 2:	Calculate the initial elastic strains on the cross section Determine: $f_{cgp}(t_{n-1})$
Step 3:	Calculate the initial elastic strains on the cross section $\Delta f_{pLT}(t_{n-1}, t_n) = \Delta f_{pSH}(t_{n-1}, t_n) + \Delta f_{pCR}(t_{n-1}, t_n) + \Delta f_{pRE}(t_{n-1}, t_n)$
Step 4:	Calculate elastic rebound due to prestress loss $\Delta f_{c,loss}(t_{n-1}, t_n) = \Delta f_{pLT}(t_{n-1}, t_n) A_{ps} \left( \frac{1}{A_g} + \frac{e_p^2}{I_g} \right)$ $\Delta f_{p,rebound}(t_{n-1}, t_n) = \Delta f_{c,loss}(t_{n-1}, t_n) \frac{E_p}{E_c(t_{n-1})}$ $\Delta f_{p,step}(t_{n-1}, t_n) = \Delta f_{pLT}(t_{n-1}, t_n) - \Delta f_{p,rebound}(t_{n-1}, t_n)$
Step 5:	Determine creep-producing forces for the start of the next step $f_p(t_n) = f_p(t_{n-1}) - \Delta f_{p,step}(t_{n-1}, t_n)$
Repeat:	Return to Step 1 with new strand stress

Each of these methods are explained in detail in the ACI 423.10 document currently under development.

The  $E/M$  using each of the three methods for each series is shown in Fig. 11. All of the methods performed similarly, with  $E/M$  between 0.76 and 1.01 and an average of 0.85. The three methods have a similar theoretical basis, so it was expected they would produce similar results.

Four different methods are mentioned by ACI 423.10 for the estimation of long-term prestress loss, two of which are considered simplified, lump-sum approaches (PCI-Simplified,<sup>21</sup> shown in Table 6, and AASHTO-Approximate,<sup>18</sup> shown in Table 7) and two being more detailed analyses (AASHTO-Detailed,<sup>18</sup> shown in Table 8, and Incremental Time-Step shown in Table 9). Each of these procedures are described in detail in ACI 423.10 with design examples. A summary of the  $E/M$  using all four of the estimation methods for specimens in each of the series is shown in Fig. 12. All of the loss-estimation procedures require the ambient relative humidity as an input variable, so the specimens within each series are subdivided based on storage location.

First comparing the two simplified procedures in Fig. 12(a), the PCI simplified method is significantly more conservative than the AASHTO approximate approach, with an average  $E/M$  of 2.38 compared to 1.27. The  $E/M$  using the PCI simplified approach are similar for the beams

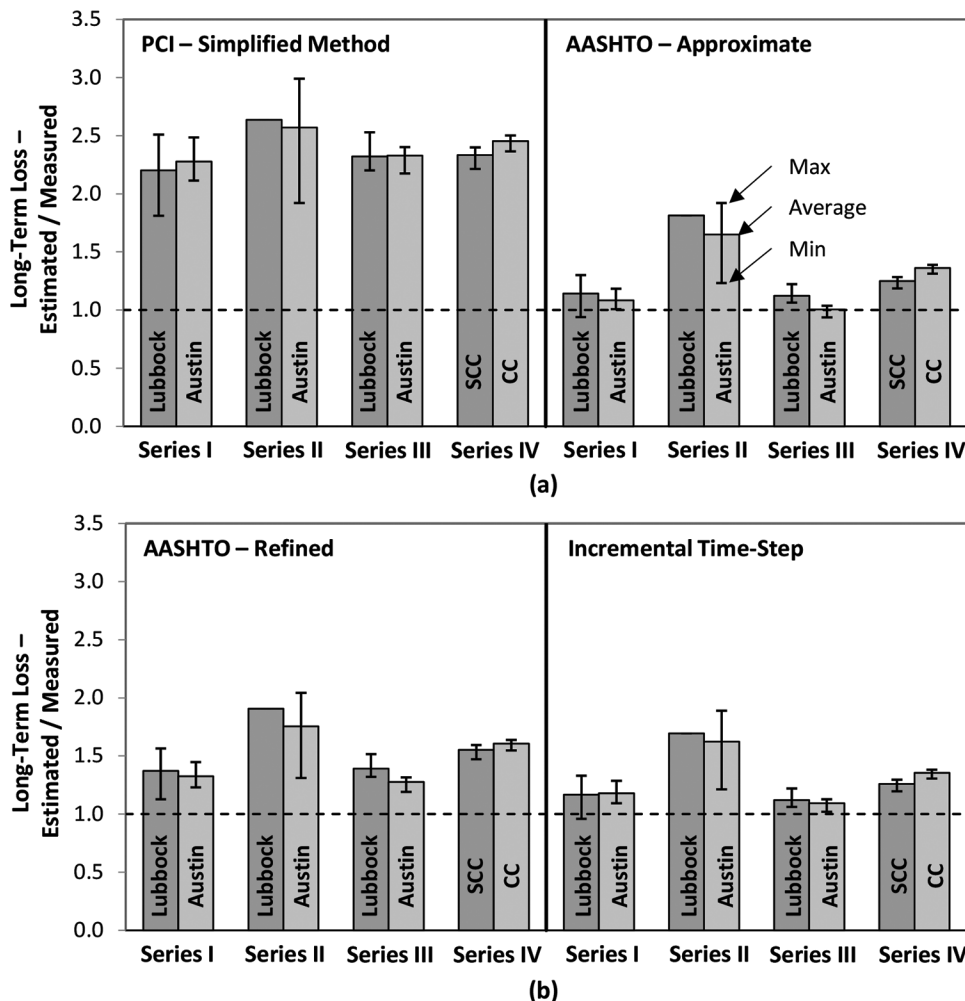


Fig. 12— $E/M$  for long-term losses measured in each series using both (a) simplified methods; and (b) detailed methods.

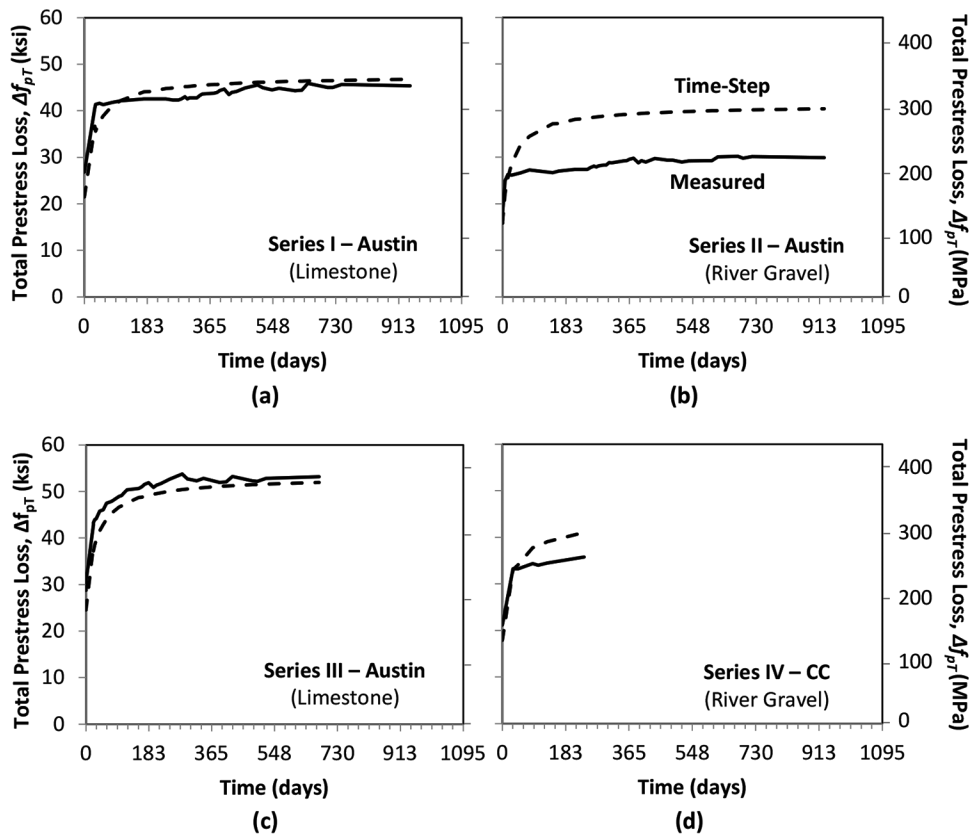


Fig. 13—Time-step analysis results compared to measured prestress loss over time for girders stored in Austin: (a) Series I; (b) Series II; (c) Series III; and (d) Series IV (CC specimens only).

constructed with softer limestone coarse aggregate (Series I and III) compared to those with stiffer river gravel coarse aggregate (Series II and IV). Using the AASHTO approximate method, the  $E/M$  for Series II and IV is noticeably higher than Series I and III. Comparison of the beams stored in Lubbock versus those in Austin reveals that both methods reasonably account for relative humidity effects.

Results from the two detailed procedures are presented in Fig. 12(b). Both the AASHTO refined and incremental time step methods offer accurate prestress loss estimates for the beams investigated in this research, with  $E/M$  of 1.49 and 1.29, respectively. The accuracy of both detailed methods is dramatically improved when compared to the PCI simplified approach. The performance of the AASHTO approximate method is similar to both detailed approaches.

One of the main advantages of both the AASHTO detailed method and the incremental time step method is the ability to estimate the development of loss over time. The time-step analysis conducted for this research was completed using the creep and shrinkage models found in the 2012 AASHTO LRFD Bridge Design Specification.<sup>18</sup> A model to represent the concrete strength over time was developed based on the measured compressive strengths obtained from cylinder testing for each series. A sample of the time-step analysis results plotted with prestress loss measured using VWGs is shown in Fig. 13. Only beams stored in Austin made with conventional concrete are presented, but the trends observed in these beams also held true in those stored in Lubbock and constructed with self-consolidating concrete.

The incremental time-step analysis offers an excellent estimate of both the loss development and the final loss for the specimens constructed with the softer limestone coarse aggregate in Series I and III. For the specimens constructed with the stiffer river gravel coarse aggregate in Series II and IV, the time-step analysis conservatively estimates the prestress loss.

## SUMMARY AND CONCLUSIONS

The purpose of this research was to 1) experimentally investigate the effect of various parameters on the development of prestress loss; 2) evaluate various methods for monitoring and measuring prestress loss; and 3) analyze the performance of various prestress loss estimation procedures. The objectives were completed through the construction, instrumentation, conditioning, monitoring, and testing of 30 full-scale bridge girders. From the experimental program, several observations and conclusions can be made, some of which confirm previous knowledge on prestress loss, and extend observations made at a material behavior level to the performance of beams:

1. The majority of prestress loss occurs within the first 4 months: The prestress loss was found to develop logarithmically, resulting in 90% of the 1-year prestress loss developing within the first 4 months after casting.

2. Relative humidity may influence prestress loss: Relative humidity was found to influence the development of loss for two out of the three series in which beams were stored in differing climates. The beams for these two series were both

cast using softer limestone coarse aggregate, which may have affected the permeability of the concrete.

3. Concrete stiffness influences prestress loss: The concrete stiffness was found to be strongly dependent on the coarse aggregate type and content, which in turn greatly affected the magnitude and development rate of prestress loss. A larger quantity of a stiff aggregate will generally result in a stiffer concrete and smaller prestress loss.

4. Prestress loss can be accurately measured using both flexural service load testing and internal instrumentation: Within the experimental program, prestress losses were measured using VWGs and flexural service load testing. Losses measured using VWGs were comparable to those measured using flexural service load testing and a stiffness based method for determining the point of first cracking.

5. Current loss procedures are available to offer conservative or accurate loss estimation: Three different elastic shortening estimation methods and four different long-term loss estimation methods were investigated. A properly calibrated time-step method was generally found to accurately model the development of prestress loss over time. The PCI-Simplified approach offered consistently conservative loss estimations. Both the AASHTO-Approximate and AASHTO-Detailed methods produced fairly accurate loss estimates for the specimens in this study.

#### AUTHOR BIOS

*ACI member David B. Garber is an Assistant Professor at Florida International University, Miami, FL. He received his BS from the Johns Hopkins University, Baltimore, MD, and his MS and PhD from the University of Texas at Austin, Austin, TX. His research interests include plasticity in structural concrete and behavior of prestressed concrete members. He is a member of Joint ACI-ASCE Committees 423, Prestressed Concrete, and 445, Shear and Torsion.*

*ACI member José M. Gallardo is an Adjunct Professor at the Technological University of Panama, Panamá, Panama. He received his BS and MS from the Technological University of Panama and his PhD from the University of Texas at Austin. His research interests include time-dependent behavior of concrete and monitoring of prestress concrete members.*

*Dean J. Deschenes is the Laboratory Manager at Simpson Gumpertz & Heger's Boston, MA, office. He received his BS from Lehigh University, Bethlehem, PA, and his MS from the University of Texas at Austin.*

*Oguzhan Bayrak, FACI, is a Professor in the Department of Civil, Environmental, and Architectural Engineering and holds the Charles Elmer Rowe Fellowship in Engineering at the University of Texas at Austin, where he serves as Director of the Phil M. Ferguson Structural Engineering Laboratory. He is a member of ACI Committees 341, Earthquake-Resistant Concrete Bridges, and S803, Faculty Network Coordinating Committee; and Joint ACI-ASCE Committees 441, Reinforced Concrete Columns, and 445, Shear and Torsion.*

#### ACKNOWLEDGMENTS

The authors would like to thank the Texas Department of Transportation for their financial support and collaborative efforts through the course of this project. The authors would like to thank the Precast Concrete Manufacturers' Association of Texas (specifically Bexar Concrete Works, Texas Concrete Works, and Valley Prestress Products) for assisting in specimen construction. The authors would also like to thank B. Stasney, A. Valentine, D. Fillip, D. Braley, and the rest of the support staff at the Ferguson Struc-

tural Engineering Laboratory for their assistance during testing of these specimens.

#### REFERENCES

1. Gallardo Méndez, J. M., "Model of Strain-Related Prestress Loss in Pretensioned Simply Supported Bridge Girders," PhD dissertation, the University of Texas at Austin, Austin, TX, 2013, 330 pp.
2. Garber, D.; Gallardo, J.; Deschenes, D.; Dunkman, D.; and Bayrak, O., "Effect of New Prestress Loss Estimates on Pretensioned Concrete Bridge Girder Design," *Report No. FHWA/TX-12/0-6374-2*, Center for Transportation Research, the University of Texas at Austin, Austin, TX, 2013, 300 pp.
3. Neville, A. M.; Dilger, W. H.; and Brooks, J. J., *Creep of Plain and Structural Concrete*, Construction Press, 1983, 380 pp.
4. Tadros, M. K.; Al-Omaishi, N.; Seguirant, S. J.; and Gallt, J. G., "Prestress Losses in Pretensioned High-Strength Concrete Bridge Girders," *NCHRP Report 496*, Transportation Research Board, Washington, DC, 2003, 73 pp.
5. Bazant, Z. P., and Wittmann, F. H., *Creep and Shrinkage in Concrete Structures*, Wiley & Sons, New York, 1982.
6. Juenger, M. C. G., and Jennings, H. M., "Examining the Relationship between the Microstructure of Calcium Silicate Hydrate and Drying Shrinkage of Cement Pastes," *Cement and Concrete Research*, V. 32, No. 2, 2002, pp. 289-296. doi: 10.1016/S0008-8846(01)00673-1
7. Mindess, S.; Young, J.; and Darwin, D., *Concrete*, Prentice Hall, Upper Saddle River, NJ, 2002, 644 pp.
8. Powers, T., "The Thermodynamics of Volume Change and Creep," *Matériaux et Construction*, V. 1, No. 6, 1968, pp. 487-507. doi: 10.1007/BF02473638
9. Tazawa, E. I.; Sato, R.; Sakai, E.; and Miyazawa, S., "Work of JCI Committee on Autogenous Shrinkage," *International RILEM Workshop on Shrinkage of Concrete (Shrinkage 2000)*, V. Baroghel-Bouny and P.-C. Aïtcin, eds., RILEM, Bagneux, France, 2000, pp. 21-40.
10. Bazant, Z. P.; Hauggaard, A. B.; Baweja, S.; and Ulm, F.-J., "Micro-prestress-Solidification Theory for Concrete Creep. I: Aging and Drying Effects," *Journal of Engineering Mechanics*, V. 123, No. 11, 1997, pp. 1188-1194. doi: 10.1061/(ASCE)0733-9399(1997)123:11(1188)
11. Hansen, T. C.; Radjy, F.; and Sellevold, E. J., "Cement Paste and Concrete," *Annual Review of Materials Science*, V. 3, No. 1, 1973, pp. 233-268. doi: 10.1146/annurev.ms.03.080173.001313
12. Ulm, F.; Le Maou, F.; and Boulay, C., "Creep and Shrinkage of Concrete—Kinetics Approach," *The Adam Neville Symposium: Creep and Shrinkage—Structural Design Effects*, SP-194, A. Al-Manaseer, ed., American Concrete Institute, Farmington Hills, MI, 2000, pp. 135-154.
13. Vandamme, M., and Ulm, F.-J., "Nanogranular Origin of Concrete Creep," *Proceedings of the National Academy of Sciences of the United States of America*, V. 106, No. 26, 2009, pp. 10552-10557. doi: 10.1073/pnas.0901033106
14. Magura, D. D.; Sozen, M. A.; and Siess, C. P., "A Study of Stress Relaxation in Prestressing Reinforcement," *Civil Engineering Studies SRS-237*, University of Illinois, Urbana, IL, 1962, 116 pp.
15. ACI Committee 318, "Building Code Requirements for Structural Concrete (ACI 318-14) and Commentary," American Concrete Institute, Farmington Hills, MI, 2014, 520 pp.
16. Birrcher, D. B.; Bayrak, O.; and Kreger, M. E., "Effects of Increasing Allowable Compressive Stress at Prestress Transfer," *ACI Structural Journal*, V. 107, No. 1, Jan.-Feb. 2010, pp. 21-31.
17. TxDOT, "Standard Specification for Construction and Maintenance of Highways, Streets, and Bridges," Texas Department of Transportation, Austin, TX, 2012.
18. AASHTO, "AASHTO LRFD Bridge Design Specification, Customary U.S. Units, 6th Edition," American Association of State Highway and Transportation Officials, Washington, DC, 2012, 1925 pp.
19. Brooks, J., "30-Year Creep and Shrinkage of Concrete," *Magazine of Concrete Research*, V. 57, No. 9, 2005, pp. 545-556. doi: 10.1680/macr.2005.57.9.545
20. Mokhtarzadeh, A., and French, C., "Time-Dependent Properties of High-Strength Concrete with Consideration for Precast Applications," *ACI Materials Journal*, V. 97, No. 3, May-June 2000, pp. 263-271.
21. PCI, *PCI Design Handbook*, seventh edition, Precast and Prestressed Concrete Institute, Chicago, IL, 2010, 804 pp.